

Comparison Between Large-Eddy Simulation and Reynolds-Averaged Navier–Stokes Computations for the MUST Field Experiment. Part I: Study of the Flow for an Incident Wind Directed Perpendicularly to the Front Array of Containers

J. L. Santiago · A. Dejoan · A. Martilli · F. Martin · A. Pinelli

Received: 22 December 2008 / Accepted: 21 January 2010
© Springer Science+Business Media B.V. 2010

Abstract The large-eddy simulation (LES) and Reynolds-averaged Navier–Stokes (RANS) methodologies are used to simulate the air flow inside the container’s array geometry of the Mock Urban Setting Test (MUST) field experiment. Both tools are assessed and compared in a configuration for which the incident wind direction is perpendicular to the front array. The assessment is carried out against available wind-tunnel data. Effects of including small geometrical irregularities present in the experiments are analysed by considering LES and RANS calculations on two geometries: an idealized one with a perfect alignment and an identical shape of the containers, and a second one including the small irregularities considered in the experiment. These effects are assessed in terms of the local time-mean average and as well in terms of spatial average properties (relevant in atmospheric modelling) given for the velocity and turbulent fields. The structural flow properties obtained using LES and RANS are also compared. The inclusion of geometrical irregularities is found significant on the local time-mean flow properties, in particular the repeated flow patterns encountered in a perfect regular geometry is broken. LES and RANS provide close results for the local mean streamwise velocity profiles and shear-stress profiles, however the LES predictions are closer to the experimental values for the local vertical mean velocity. When considering the spatial average flow properties, the effects of geometrical irregularities are found insignificant and LES and RANS provide similar results.

Keywords Flow around array of obstacles · Large-eddy simulation · MUST experiment · Reynolds-averaged Navier–Stokes

J. L. Santiago (✉) · A. Martilli · F. Martin
Environment Department, Research Center for Energy, Environment and Technology (CIEMAT),
Av. Complutense 22, 28040 Madrid, Spain
e-mail: jl.santiago@ciemat.es

A. Dejoan · A. Pinelli
Energy Department, Research Center for Energy, Environment and Technology (CIEMAT),
Av. Complutense 22, 28040 Madrid, Spain

 Springer

21 **1 Introduction**

22 Air quality is of growing concern in the urban environment and an accurate prediction of
23 transport and dispersion of contaminants is needed. However, the complex surface morphol-
24 ogy (buildings and other obstacles) that forms the urban canopy makes difficult the study
25 of such a physical process. The interaction between the atmospheric turbulent boundary
26 layer and the urban geometry generates complex flow patterns that determine the distri-
27 bution of urban pollutant concentrations. Measurements of the dispersion of pollutants in
28 urban areas or around obstacles have been carried out in several wind-tunnel or water-tun-
29 nel experiments (e.g., Meroney et al. 1996; Pavageau and Schatzmann 1999; Kastner-Klein
30 and Plate 1999; Cheng and Castro 2002; Castro et al. 2006; Yee et al. 2006) and also in
31 field experiments (e.g., Biltoft 2001; Dobre et al. 2005). Simple models such as Gaussian
32 plume models, widely used in application for simple terrain, perform poorly for the pre-
33 diction of urban environment dispersion because the complex geometry formed by bluff
34 bodies such as buildings has to be explicitly modelled to correctly represent the interaction
35 between the urban canopy and the atmospheric flow. Details of the flow around buildings
36 can be tackled using the computational fluid dynamics (CFD) approach, which has been
37 extensively used in simulations of dispersion phenomena in urban regions during this last
38 decade. An “exact” numerical approach would rely upon the use of direct numerical simu-
39 lation (DNS), where all the scales of the turbulence motion are resolved, thus allowing for
40 obtaining very detailed information on the flow field. However, due to its computational cost,
41 DNS is still restricted to the study of turbulent flow around an isolated building or around
42 a limited number of obstacles (Yakhov et al. 2006; Coceal et al. 2006). On the other hand,
43 the Reynolds-averaged Navier–Stokes (RANS) approach considers an integral approach for
44 the whole turbulence spectrum so that turbulence modelling assumptions are required for
45 the statistical closures. This approach does not require large computing resources and is the
46 most commonly used. For example, Kim and Baik (2004), Santiago et al. (2007), and Milliez
47 and Carissimo (2007) made use of RANS for the calculation of flow over idealized urban
48 geometries while Flaherty et al. (2007) and Michioka and Sato (2009) carried out RANS
49 simulations over real urban geometries. An intermediate approach is the large-eddy simu-
50 lation (LES) methodology, which, by means of a spatial filtering operation applied to the
51 Navier–Stokes equations, resolves explicitly the dynamics of the unsteady large scales of
52 turbulence while modelling the effect of small-scale motions on the resolved ones. Applica-
53 tion of LES in the urban environment has been pursued by Hanna et al. (2002), Cheng et al.
54 (2003), and Xie and Castro (2006) in flows over an array of regular cubes and by Camelli
55 et al. (2005) and Tseng et al. (2006) and very recently by Michioka and Sato (2009) and Xie
56 and Castro (2009) in field scale flows. Potentially, the capabilities of LES for the simulation
57 of urban dispersion are superior to RANS; however, its applicability is more problematic due
58 to the large computing time required (unsteady three-dimensional fields must be considered)
59 compared to RANS and also to some issues regarding the implementation of wall and inlet
60 conditions.

61 Comparative studies between RANS and LES approaches for flows over urban geome-
62 tries are scarcely available. Cheng et al. (2003) compared the air flow computed by LES and
63 RANS models over an array of cubes and found that both LES and RANS methodologies
64 predicted reasonably well the main characteristics of the mean flow. They also stressed that,
65 for their study, the LES computational cost was approximately 100 times greater than RANS.
66 Xie and Castro (2006) showed that RANS and LES provide comparable results above the
67 canopy layer of a flow over a staggered array of cubes, although the details of the field within
68 the canopy were better captured by LES.

69 Even if CFD models can be applied successfully to simulate the flow over the complex
70 morphology of a city, they present some limitations regarding their computational cost and
71 can thus not be easily applied to air quality studies that include the whole city and its sur-
72 roundings. In this case, numerical atmospheric models with simplified urban canopy models
73 are most commonly used in order to catch the mesoscale features. In this context, the urban-
74 obstacle effects within the canopy layer must be parameterised. Several parameterisations
75 based on a horizontally-averaged approach have been recently proposed (Martilli et al. 2002;
76 Coceal and Belcher 2004) for the modelling of the urban canopy. However, the validation of
77 the parameterisation is still a difficult issue due to the lack of information on the spatially-
78 averaged variables required for the parameterisation itself. In this context, CFD models can
79 be a useful tool to provide flow variables with high enough spatial resolution to compute
80 accurate values of the spatially-averaged properties over zones that are comparable to the
81 grid-cell volume used in mesoscale models. Martilli and Santiago (2007) and Santiago et al.
82 (2008) made use of the RANS approach for obtaining spatially-averaged flow properties in
83 their parameterisation study of flow over an idealized urban geometry. The spatially-averaged
84 flow properties were also extracted from DNS data by Coceal et al. (2006) for a simplified
85 geometry.

86 A very interesting field experiment for urban environment dispersion simulation purposes
87 is the Mock Urban Setting Test (MUST) experiment set up in the Great Desert (USA) to
88 investigate the dispersion of a passive scalar within an array of containers (Biltoft 2001).
89 This flow configuration was also studied in wind-tunnel and water-channel experiments (Yee
90 et al. 2006; Leitl et al. 2007). Moreover, with its relatively simple geometry, it has also
91 been extensively used for the evaluation of urban CFD models, using RANS (Milliez and
92 Carissimo 2007; Di Sabatino et al. 2009) and, to a lesser extent, employing LES (Camelli
93 et al. 2005).

94 In the present study we apply both LES and RANS methodologies to simulate the MUST
95 experiment. Our study is divided into two parts. In this Part I we focus on the comparisons
96 of the flow properties obtained with RANS and LES and propose the following:

- 97 (1) Establish a comparison methodology between RANS and LES performed in the limit of
98 the grid resolution that ensures that the large building-scale flow is reasonably resolved.
99 The minimum grid resolution required to obtain acceptable predictions using LES for
100 the flow in an urban environment is not well established. The grid resolution used here
101 lies between the requirements given by Tseng et al. (2006) and by Xie and Castro (2006).
102 This kind of comparison is particularly significant for practical applications, if the dif-
103 ference in computing costs between the two modelling approaches is considered. The
104 comparison between LES and RANS proposed here is based on two flow-scale levels:
105 the local microscale (urban-street flow scales), relevant to the dispersion patterns within
106 the urban canopy, and the mesoscale (extracted from the spatially-averaged flow prop-
107 erties), relevant to the development and validation of urban-layer parameterisation in
108 atmospheric modelling.
- 109 (2) Establish the effects of small irregularities upon the flow within an array of urban-like
110 obstacles. This is significant, for example, if we want to generalize results obtained for
111 a specific configuration (idealized or real) to other similar but simplified configurations.
112 Part of the numerical investigations that focus upon the MUST flow configuration does
113 not include the small topological irregularities (different size of containers and not per-
114 fect alignment of the containers within the array) in the calculations (Yee et al. 2006;
115 Milliez and Carissimo 2007) while others take them into account (Camelli et al. 2005;
116 Di Sabatino et al. 2009). In general, the effects of their inclusion or omission on the

117 local microscale and on spatially-averaged flow properties were not discussed in these
118 previous studies.

119 These issues are addressed here by considering two geometries when modelling the MUST
120 flow configuration with the upstream flow directed perpendicular to the front array of the
121 containers: a first geometry has the containers of identical size and perfectly aligned within
122 the array, and a second realistic geometry includes the small irregularities present in the
123 MUST field experiment. The wind-tunnel experimental data of [Bezpalcova \(2007\)](#) are used
124 as a reference for our comparative study.

125 The paper is organised as follows: In Sect 2, a brief description of the MUST experiment
126 is given, and the computational settings are described in Sect. 3. The results are presented
127 in Sect. 4 and ordered as follows: first a comparison between RANS, LES and wind-tunnel
128 measurements based on a statistical analysis is given in Sect. 4.1; secondly, the comparisons
129 based on the local mean flow velocity and Reynolds shear stress is carried out by analysing
130 the small geometrical irregularity effects in Sect. 4.2; in Sect. 4.3, this comparative analysis
131 is provided for the spatially-averaged flow properties. Finally some concluding remarks are
132 given in Sect. 5.

133 A comparative study of RANS and LES approaches for the simulation of passive contam-
134 inant dispersion in the MUST field experiment configuration is presented in Part II ([Dejoan
135 et al. 2010](#)).

136 2 Brief Description of the MUST Experiment

137 The MUST field experiment was conducted in September 2001 at the Horizontal Grid, U.S.
138 Army Dugway Proving Ground (DPG) by the Defence Threat Reduction Agency (DTRA).
139 Many research agencies and universities have collaborated in the development of this exper-
140 iment: U.S. Army Atmospheric Research Laboratory, Canadian Defence Research Estab-
141 lishment Suffield (DRES), UK Defence Science and Technology Laboratory (DSTL), U.S.
142 Department of Energy (DOE), Los Alamos National Laboratory (LANL), Arizona State
143 University (ASU) and the University of Utah. The experiment was designed to study the
144 dispersion of a tracer through a large array of obstacles, to overcome the scaling constraints
145 and measurement limitations of laboratory experiments and to obtain datasets at a near real-
146 istic scale useful for urban dispersion modelling ([Biltoft 2001](#)). A 12×10 aligned array of
147 shipping containers was used to simulate the urban environment. Each container was 12.2 m
148 long, 2.42 m wide and 2.54 m height, except for the one identified as H5, which was 6.1 m
149 long, 2.44 m wide and 3.51 m height. In addition, the configuration of the array is slightly
150 irregular due to several alignment errors. The average obstacle spacing is $\langle L_x \rangle / h = 5.08$
151 in the lengthwise direction (x -direction) and $\langle L_y \rangle / h = 3.11$ in the span-wise direction (y -
152 direction), where h is the height of the standard container. A plan view of the irregular array
153 is shown in Fig. 1. The array forms an angle of 30° to the north. The experimental set-up is
154 described in detail in [Biltoft \(2001\)](#) and [Yee and Biltoft \(2004\)](#). Similar measurements with
155 the same configuration (including the geometrical irregularities) were performed in the wind
156 tunnel of the University of Hamburg within a scaled model (1:75) by [Bezpalcova \(2007\)](#);
157 the flow properties were recorded using laser Doppler anemometry ([Leitl et al. 2007](#)). The
158 Reynolds numbers, $Re = U_{\text{inlet}} h / \nu$, based on the inlet velocity, U_{inlet} , the height of the
159 container, h , and the kinematic viscosity, ν , are approximately 10^6 in the field experiments
160 and 10^4 in the wind-tunnel experiments.

161 The experimental data used in the comparative analysis presented here belong to one trial
162 of the wind-tunnel experiment of [Bezpalcova \(2007\)](#) and [Leitl et al. \(2007\)](#) for which the inlet

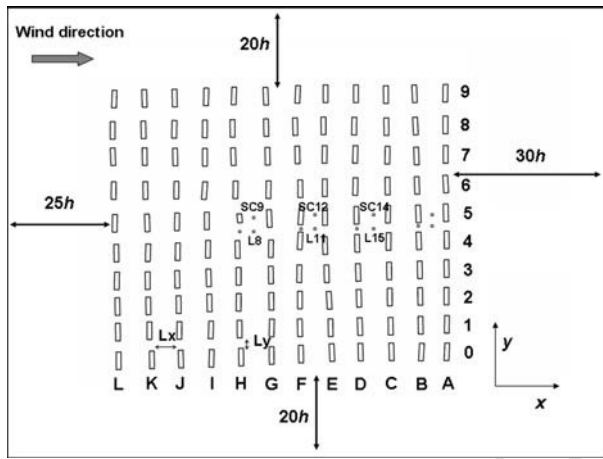


Fig. 1 Irregular array geometry: plan view of the real MUST geometry

163 flow conditions are well controlled. Here, we make use only of the flow field measurements
 164 corresponding to the case with an upstream flow impinging perpendicularly to the array of
 165 the containers. Part II (Dejoan et al. 2010) will focus upon data from the field experiment
 166 with a different wind direction.

167 3 Computational Procedure

168 3.1 Flow Equations and Numerical Methods

169 In both the LES and RANS calculations a neutral turbulent flow was considered, i.e., without
 170 including buoyancy and stratification effects. In the LES approach, the large-scale flow is
 171 described by the filtered incompressible Navier–Stokes equations,

$$172 \quad \frac{\partial \tilde{U}_i}{\partial t} + \frac{\partial \tilde{U}_j \tilde{U}_i}{\partial x_j} = -\frac{\partial \tilde{P}}{\partial x_i} + \nu \frac{\partial^2 \tilde{U}_i}{\partial x_j \partial x_j} - \frac{\partial \tau_{ij}}{\partial x_j} \quad (1)$$

173 where \tilde{U}_i , \tilde{P} define the filtered velocity component and the filtered pressure, respectively,
 174 and ν is the fluid kinematic viscosity. The contribution of the subgrid scale to the resolved
 175 flow variables, represented by the stress tensor τ_{ij} , is modelled by the standard Smagorinsky
 176 model (Smagorinsky 1963)

$$177 \quad \tau_{ij} = -2\nu_{sgs} \tilde{S}_{ij} = (C_s \Delta)^2 |\tilde{S}| \tilde{S}_{ij} \quad (2)$$

178 where $\tilde{S}_{ij} = 0.5(\partial \tilde{U}_i / \partial x_j + \partial \tilde{U}_j / \partial x_i)$ is the filtered strain tensor and ν_{sgs} is the subgrid-scale
 179 viscosity. The Smagorinsky constant C_s is set to a value of 0.1 and the filter width, Δ , is
 180 deduced from the grid computational size. Due to its simplicity and low computational cost,
 181 the Smagorinsky subgrid-scale model is at the moment the most commonly used in LES flow
 182 for urban-like geometry (Xie and Castro 2006, 2009).

183 The LES simulations were performed using as a baseline code the open source CFD code
 184 OpenFoam (2006). The numerical method incorporated in this package to discretize Eqs.

1 and 2 is based on the finite volume method formulated in a collocated grid arrangement. A Pressure Implicit Splitting of Operators (PISO) algorithm with two corrector steps is used to couple the velocity and the pressure. An incomplete-Cholesky preconditioned bi-conjugate gradient algorithm is used to solve the linearised equations of the velocity components while an algebraic multi-grid solver is used for the discretised pressure Poisson equation. A Rhie–Chow interpolation is used for the pressure gradient terms to avoid pressure oscillations due to the collocated grid arrangement. The temporal integration is performed by using the second-order semi-implicit backward scheme and the spatial derivatives are discretised according to the second-order central differencing scheme.

The RANS calculations were carried out by making use of FLUENT code (Fluent Inc. 2005) to solve the steady incompressible RANS equations; the turbulence closure used is the standard k – ε model. The governing equations are:

$$\bar{U}_j \frac{\partial \bar{U}_i}{\partial x_j} = -\frac{1}{\rho} \frac{\partial \bar{P}}{\partial x_i} + \frac{\mu}{\rho} \frac{\partial^2 \bar{U}_i}{\partial x_j \partial x_j} - \frac{\partial}{\partial x_j} (\overline{u'_i u'_j}), \quad (3)$$

$$\bar{U}_j \frac{\partial k}{\partial x_j} = \frac{1}{\rho} \frac{\partial}{\partial x_j} \left[\left(\mu + \frac{\mu_t}{\sigma_k} \right) \frac{\partial k}{\partial x_j} \right] + \frac{G_k}{\rho} - \varepsilon, \quad (4)$$

$$\bar{U}_j \frac{\partial \varepsilon}{\partial x_j} = \frac{1}{\rho} \frac{\partial}{\partial x_j} \left[\left(\mu + \frac{\mu_t}{\sigma_\varepsilon} \right) \frac{\partial \varepsilon}{\partial x_j} \right] + \frac{1}{\rho} C_{\varepsilon 1} G_k \frac{\varepsilon}{k} - C_{\varepsilon 2} \frac{\varepsilon^2}{k}, \quad (5)$$

where k is the turbulent kinetic energy and ε is the dissipation rate of turbulent kinetic energy, μ is the dynamic viscosity, $-\overline{u'_i u'_j} = \frac{1}{\rho} \mu_t \left(\frac{\partial \bar{U}_i}{\partial x_j} + \frac{\partial \bar{U}_j}{\partial x_i} \right) - \frac{2}{3} k \delta_{ij}$ is the Reynolds stress, μ_t is the turbulent viscosity expressed as $\mu_t = \rho C_\mu \frac{k^2}{\varepsilon}$, G_k is the turbulent kinetic energy production, σ_k ($= 1.0$) and σ_ε ($= 1.3$) are the turbulent Prandtl numbers for k and ε , respectively, the model constants C_μ , $C_{\varepsilon 1}$ and $C_{\varepsilon 2}$ take the respective standard values 0.09, 1.44 and 1.92 that were used for a wide range of turbulent flows (Lauder and Spalding 1974; Versteeg and Malalasekera 1995). Note that in LES the Reynolds shear stress is a direct output of the simulation while in RANS it is fully modelled (see above relation).

The RANS governing equations are solved in a collocated grid system using a finite volume method. The pressure–velocity coupling is solved by means of the semi-implicit method for pressure-linked equations algorithm (SIMPLE) (Patankar 1980). A second-order upwind scheme is used for the discretisation of the advection terms.

3.2 Computational Set-Up

3.2.1 Flow Geometries and Parameters

In our simulations, two geometry configurations were taken into account: the first geometry is composed of an array of containers all having identical size and shape and perfectly aligned. The second geometry considered includes the irregularities of the MUST experiment configuration. Note that in the wind-tunnel experiment the MUST scaled model also contains the geometrical irregularities. These two flow configurations will be referred to as “the regular array case” and “the irregular array case”, respectively. An overview of these geometries is given in Figs. 1 and 2.

In the regular array case, the computational domain was limited to a few rows of containers of the MUST geometry. As shown in Figs. 2a and b, the RANS regular array was composed of five rows of 12 containers while the LES domain includes three rows of eight containers.

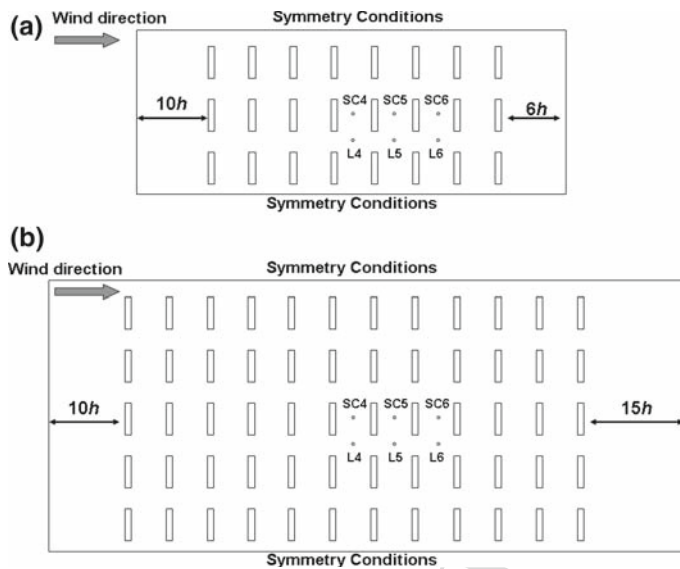


Fig. 2 Regular array geometry: plan view of the simplified MUST configuration, a LES and b RANS

224 At the lateral boundaries of the domain, symmetry conditions were applied, which is
 225 equivalent to simulating an infinite array of containers in the span-wise direction. This re-
 226 duced computational domain allows us to perform calculations with a relative fine resolution
 227 at reasonable computing costs (in particular for LES) and can be justified by the experi-
 228 mental study of Meinders and Hanjalic (1999) who observed that flow patterns repeat along
 229 the streamwise and span-wise directions inside a regular array of obstacles. Note that, the
 230 regular array of containers presents the same average geometry characteristics as the field
 231 experiment geometry. In the irregular case, the computational domain covers the full MUST
 232 array (12 × 10 containers) and includes the small non-alignment and small variations in size
 233 and shape of the containers (see Fig. 1).

234 The upper limit of the domain is located both for LES and RANS at 11h in the regular
 235 case and at 8h in the irregular case. The extensions of the domain in the streamwise and
 236 lateral directions are given for each geometry in Figs. 1 and 2.

237 The Reynolds number, based on the inlet velocity, U_{inlet} , the height of the container, h ,
 238 and the kinematic viscosity, ν , is set to $Re = U_{inlet}h/\nu = 4,700$ in the regular array case
 239 and to $Re = 10^6$ in the irregular array one. Note that, for the irregular geometry, the Rey-
 240 nolds number used is the same as that in the field experiment while in the regular geometry
 241 the Reynolds number is approximately half that in the wind-tunnel experiment. Both Rey-
 242 nolds numbers satisfy the criterion ($Re > 4,000$) given by Snyder (1981) and by Castro
 243 and Robins (1997) for Reynolds-number independency in the physical modelling of flows
 244 around obstacles. A more recent experimental study on the Reynolds-number-independency
 245 assumption by Lim et al. (2007) showed that, in certain circumstances (mainly related to
 246 the presence of strong vortex motion), flow quantities can be Reynolds-number dependent.
 247 However, in the present case, where the incident flow is oriented perpendicularly to the front
 248 of the obstacles, the Reynolds-number dependency is expected to be small on the mean and
 249 fluctuating velocity fields, in agreement with the results obtained by Lim et al. (2007) for
 250 the flow over a cube with an incident flow normal to the face of the cube (a significant

251 Reynolds-number dependency was only found on the fluctuating surface pressure field for
 252 this configuration).

253 3.2.2 Grid Resolution

254 Preliminary grid resolution tests were performed for flow over a single container at the
 255 Reynolds number, $Re = 10^6$. Periodic boundary conditions were applied at the streamwise
 256 and lateral edges of the single container computational domain and a free-slip condition at
 257 the top. In the periodic streamwise direction the mean flow motion was induced by apply-
 258 ing a constant streamwise mean pressure gradient in the RANS simulations and a constant
 259 flow rate in the LES. In the RANS calculations four grid tests (grids 0–3) were considered
 260 while in LES three grid tests (grids 1–3) were analyzed as given in Table 1. The influence
 261 of grid resolution for the single container configuration is shown in Fig. 3 for the profiles
 262 of the mean Reynolds shear stress at two locations about the container that corresponds to
 263 the positions SC and L indicated on Fig. 1. RANS calculations show that the shear-stress
 264 profile presents small differences between grids 1 and 2, and it is almost identical between
 265 grids 2 and 3. Grid systems 2 and 3 correspond to an increase in the number of grid cells
 266 for the discretization of the single container by a factor 8 (doubling the number of cells of
 267 grid 1 in each direction) and 64 (quadrupling the number of cells of grid 1 in each direction),
 268 respectively. At location SC the shear-stress profiles almost collapse while at location L some
 269 grid dependency is observed. Nevertheless, at this location the shear stress is low and the
 270 grid effects are not significant. Regarding the LES, the shear-stress profile varies a little from
 271 grids 1 to 3, especially at location SC where all profiles are very similar. At location L, the
 272 shear stress is identical in grids 1 and 2 but shows a higher peak in grid 3. Note that RANS
 273 shear-stress profiles exhibit a different shape than LES and that the peak value of the shear
 274 stress is higher in RANS than in LES. Beside the difference in the modelling approach, this
 275 may be in part explained by the different driving force methods used to maintain the mean
 276 flow in the periodic streamwise direction (in RANS a constant mean streamwise pressure
 277 gradient is used, while in LES the mean flow is sustained by forcing directly the mean flow
 278 rate to be constant). The RANS and LES velocity profiles showed a similar grid-resolution
 279 influence as for the respective shear stress (not shown here). For the RANS simulations, only
 280 grid 0 (coarsest grid) gives strong differences in the streamwise velocity predictions. Since
 281 the differences observed in the flow quantities, when comparing grids 1 and 2, are small and
 282 for the sake of keeping reasonable computing time (in particular for the LES) the number of
 283 grid points across the buildings used for the simulations of the full irregular case domain was
 284 kept as in grid 1 ($11 \times 4 \times 10$) for both RANS and LES simulations. In the regular case the
 285 computational domain is smaller than in the irregular case, which allowed for more savings
 286 regarding computing time and to make use of a little more refined grid resolution than grid 1
 287 in RANS ($15 \times 5 \times 10$) and LES ($16 \times 5 \times 12$). The grids used in the present LES are between
 288 the requirements given by Tseng et al. (2006) (6 grid points per edge) and Xie and Castro
 289 (2006) (20 grid points per edge) to reasonably resolve the flow over cuboid-shape obstacles
 290 with LES. Note that making use of grid 3 in LES would lead to a quite extensive usage of
 291 computing time, a factor of about 20 approximately compared to grid 1. We recall here that
 292 our purpose is to make use of LES to resolve reasonably well the large scales dictated by
 293 the building sizes while keeping an affordable computational cost as compared to the RANS
 294 requirements. The energy spectra obtained using LES, given in Fig. 4 for the irregular and
 295 regular geometry cases at two locations behind the containers, exhibit a limited inertial range
 296 but show that the smallest resolved flow turbulence scales are well located in the inertial
 297 subrange.

Table 1 Grid characteristics

	Regular		Irregular		Grid test 0		Grid test 1		Grid test 2		Grid test 3	
	LES	RANS	LES	RANS	LES	RANS	LES	RANS	LES	RANS	LES	RANS
Total cells	$\approx 1.1 \times 10^6$	$\approx 1.3 \times 10^6$	$\approx 1.6 \times 10^6$	$\approx 1.6 \times 10^6$	—	$\approx 1.4 \times 10^3$	$\approx 1.7 \times 10^4$	$\approx 1.3 \times 10^4$	$\approx 1 \times 10^5$	$\approx 1 \times 10^5$	$\approx 3.7 \times 10^5$	$\approx 7 \times 10^5$
Gridpoints containers length	16	15	11	11	—	6	11	11	24	22	34	44
Gridpoints containers width	5	5	4	4	—	2	4	4	8	8	12	16
Gridpoints containers height	12	10	10	10	—	5	10	10	16	20	22	40

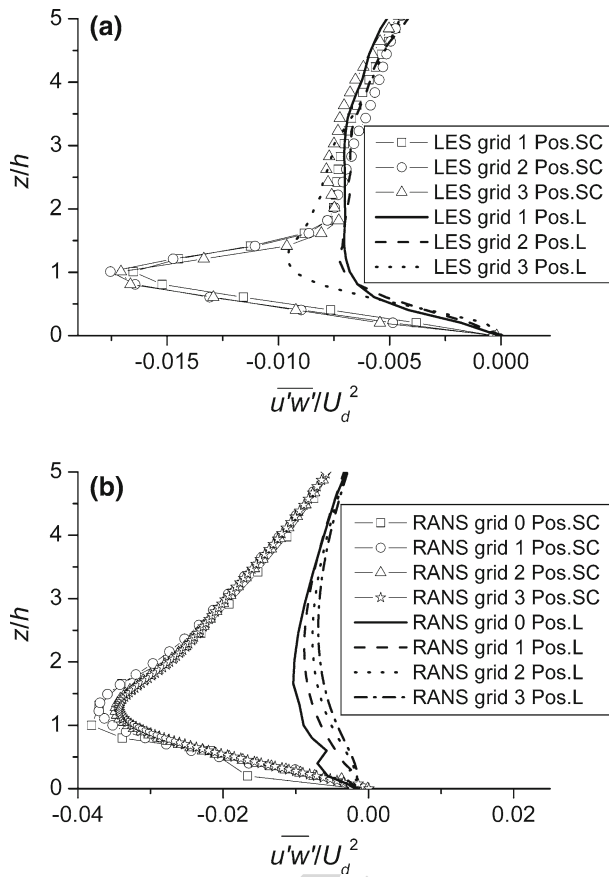


Fig. 3 Grid resolution tests over one single unit container: vertical profiles of the mean Reynolds shear stress: **a** LES simulations and **b** RANS simulations. The normalization used is by reference to the flow rate velocity, U_d . The locations SC and L are equivalent to the locations SC1–SC4 and L1–L4 around the container (see Figs. 1 and 2)

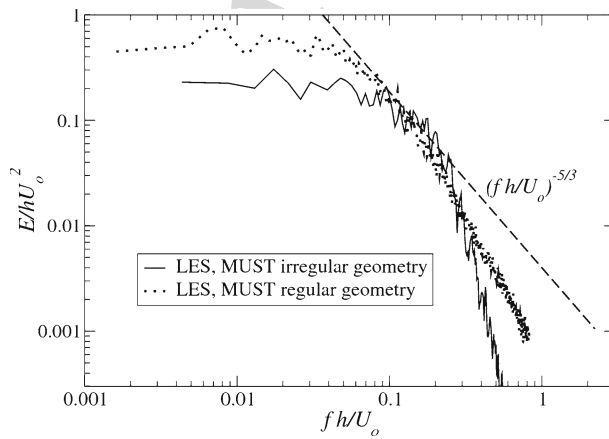


Fig. 4 Energy spectra obtained from the LES simulations of the regular and irregular cases

298 3.2.3 Boundary Conditions

299 The inflow condition applied in the RANS calculations of the regular array case is extracted
300 from a preliminary RANS simulation of a fully turbulent flow in a periodic channel whose
301 cross-section is identical to the one that contains the obstacles. The inflow velocity in the
302 irregular case is fitted from the wind-tunnel experiment data of [Bezpalcova \(2007\)](#). In both
303 regular and irregular cases, the boundary conditions applied at the walls consist of a standard
304 logarithmic type boundary condition for the tangential stresses and a zero velocity orthogonal
305 to the walls. At the top of the domains a free-slip condition is applied and at the outlet the
306 pressure is prescribed and the velocity extrapolated from a zero-gradient condition.

307 In the LES, the wall, top and outflow boundary conditions are similar to those used in
308 RANS. More recent approaches for LES wall boundary conditions in high Reynolds-number
309 flows have been developed, such as wall modelling based on turbulent boundary-layer equa-
310 tions or hybrid RANS/LES (see [Cabot and Moin 1999](#); [Nikitin et al. 2000](#); [Piomelli and
311 Ballaras 2002](#)). However, the use of a logarithmic-based wall boundary condition is the most
312 commonly used in LES for flows over buildings ([Tseng et al. 2006](#); [Xie and Castro 2006](#),
313 [2009](#)). The use of the logarithmic-type wall boundary condition is based on the fact that
314 viscous effects are negligible in such flows, the generation of turbulence being mainly asso-
315 ciated with the large flow scales produced by the presence of the obstacles. For the inflow
316 conditions, a mean velocity profile to which is added random noise is used. In the regular
317 case a uniform velocity profile was used while in the irregular case the mean profile is fitted
318 to the experimental wind-tunnel inflow data. Though not shown here, it was observed in the
319 irregular case that the shape of the mean inlet profile (i.e. uniform or with a boundary layer
320 fitted with the experimental data) has little influence on the flow quantities within the array
321 that are presented here. The LES inflow condition used here is as simple as that used by
322 [Hanna et al. \(2002\)](#) for flow within cubical obstacle arrays or by [Smorlakiewicz et al. \(2007\)](#)
323 for flow over the Pentagon building, in the sense that the time and space correlations are not
324 based on a physical content but on a random process. Only very recently, [Xie and Castro
325 \(2009\)](#) developed an inflow approach for LES of street-scale flows. This approach was not
326 considered here.

327 3.2.4 Integration Time in LES Simulations

328 The timestep used in the LES is such that the Courant number does not exceed 0.6. The
329 velocity statistics were accumulated over several “through flow” time units, $T = L_x/U_o$,
330 after having reached a satisfactory developed turbulent field. For the regular geometry case
331 the statistics were performed over a total time of $40T$, while in the case of the irregular
332 geometry a total statistical time of $15T$ was used.

333 4 Results

334 A comparison between LES, RANS and experimental data is presented for the velocity and
335 turbulence fields in the case of flow approaching the array perpendicular to the obstacles (see
336 Fig. 1). The experimental data used for validation are those obtained from the wind-tunnel
337 experiment of [Bezpalcova \(2007\)](#) and [Leitl et al. \(2007\)](#), which are the most complete data-
338 sets available for the flow quantities. The present comparison aims to gain insight into the
339 effects of introducing geometrical irregularities, and how far their inclusion is relevant for
340 the computation of such flows.

341 First, the RANS and LES results are compared with experimental data according to a
 342 statistical analysis for the irregular case only (wind-tunnel data correspond to the irregular
 343 case). Secondly, the results obtained with RANS and LES for the profiles of the mean velocity
 344 and turbulence field quantities are compared with measurements at several locations and are
 345 analysed for the regular and irregular cases. Then, information on the flow structure is given
 346 by considering the streamlines of the mean flow velocity. Finally, the results obtained for the
 347 horizontal spatially-averaged properties of flow quantities are compared in the regular and
 348 irregular cases.

349 All flow quantities are normalized by reference to the height of the obstacles, h , and the
 350 streamwise inlet velocity (U_0) taken at the height $z \approx 3h$.

351 4.1 Statistical Analysis

352 We use the wind-tunnel measurements of \bar{U} , \bar{W} and $\overline{u'w'}$ for several vertical profiles (12
 353 profiles, 317 data points) distributed inside the irregular array close to the H5, F5, D5 and
 354 B5 containers (Bezpalcova 2007; Leiti et al. 2007); the locations are indicated in Fig. 1. The
 355 experimental data cover a distance from the ground up to $5h$ approximately. The metrics used
 356 are the normalised square mean error (NMSE), fractional bias (FB), correlation coefficient
 357 (R), factor 2 (FAC2) and hit rate (q), defined as:

$$358 \quad \text{NMSE} = \frac{\sum_{i=1}^n (O_i - P_i)^2}{\sum_{i=1}^n O_i \cdot \sum_{i=1}^n P_i}, \quad (6)$$

$$359 \quad \text{FB} = \frac{\sum_{i=1}^n O_i - \sum_{i=1}^n P_i}{0.5 \cdot (\sum_{i=1}^n O_i + \sum_{i=1}^n P_i)}, \quad (7)$$

$$360 \quad R = \frac{\sum_{i=1}^n [(O_i - \frac{1}{n} \sum_{i=1}^n O_i) (P_i - \frac{1}{n} \sum_{i=1}^n P_i)]}{\left[\sum_{i=1}^n (O_i - \frac{1}{n} \sum_{i=1}^n O_i)^2 \right]^{1/2} \left[\sum_{i=1}^n (P_i - \frac{1}{n} \sum_{i=1}^n P_i)^2 \right]^{1/2}}, \quad (8)$$

$$361 \quad \text{FAC2} = \text{fraction of data that satisfy } 0.5 \leq P_i/O_i \leq 2.0, \quad (9)$$

$$362 \quad q = \frac{1}{n} \sum_{i=1}^n N_i \text{ with } N_i = \begin{cases} 1 & \text{if } |(O_i - P_i)/O_i| \leq RD \text{ or } |O_i - P_i| \leq AD \\ 0 & \text{otherwise} \end{cases} \quad (10)$$

363 where n is the total number of sample points, O_i are the measured data and P_i are the predicted
 364 values, RD and AD represent the allowed relative deviation and the allowed absolute deviation
 365 of model results from the reference data, respectively. A relative deviation of $RD = 0.25$
 366 for all variables and an absolute deviation of $AD = 0.05$ for normalised velocities (\bar{U}/U_0 ,
 367 \bar{W}/U_0) and $AD = 0.005$ for $\overline{u'w'}/U_0^2$ are used. The value of AD for normalised velocities and
 368 RD are similar to those used by Santiago et al. (2007) and Eichhorn (2004). Two analyses are
 369 made: one with the full dataset (Table 2) and the other with data corresponding to $z/h < 1$,
 370 i.e., within the canopy (110 data points, Table 3).

371 4.1.1 Hit Rate

372 The value of the hit rate for a successful validation based on the (VDI, 2005, guidelines) is
 373 $q > 66\%$. For the full dataset, all variables fulfil this q limit. However, for the dataset within
 374 the canopy ($z/h < 1$) the hit rate decreases, indicating that in this zone the models have
 375 greater difficulties simulating the flow patterns accurately. Similar findings were found for
 376 RANS by Franke et al. (2008) who showed that RANS models for the MUST configuration

Table 2 Metrics computed from RANS and LES results for the irregular case with the full experimental dataset

	Hit rate	Hit rate*	FAC2	FB	NMSE	R
\bar{U}/U_0 (RANS)	0.77	0.74	0.896	0.031	0.03	0.949
\bar{U}/U_0 (LES)	0.76	0.75	0.849	0.108	0.04	0.960
\bar{W}/U_0 (RANS)	0.81	0.24	0.204	1.500	75.64	0.901
\bar{W}/U_0 (LES)	0.83	0.25	0.449	116	-10.34	0.866
$\overline{u'w'}/U_0^2$ (RANS)	0.67	–	0.902	0.180	0.26	0.639
$\overline{u'w'}/U_0^2$ (LES)	0.81	–	0.826	0.264	0.26	0.703

Hit rate* is the hit rate corresponding to more restricted values of AD ($AD=0.008$ and 0.007 for \bar{U}/U_0 , \bar{W}/U_0)

Table 3 Metrics computed from RANS and LES results for the irregular case with the experimental dataset inside the canopy

	Hit rate	Hit rate*	FAC2	FB	NMSE	R
\bar{U}/U_0 (RANS)	0.60	0.54	0.718	0.092	0.10	0.918
\bar{U}/U_0 (LES)	0.56	0.55	0.627	0.303	0.17	0.932
\bar{W}/U_0 (RANS)	0.70	0.15	0.074	1.111	22.65	0.892
\bar{W}/U_0 (LES)	0.71	0.25	0.370	15.379	-8.55	0.865
$\overline{u'w'}/U_0^2$ (RANS)	0.57	–	0.782	0.394	0.37	0.716
$\overline{u'w'}/U_0^2$ (LES)	0.53	–	0.645	0.494	0.51	0.676

Hit rate* is the hit rate corresponding to more restricted values of AD ($AD=0.008$ and 0.007 for \bar{U}/U_0 , \bar{W}/U_0)

377 give values of q under the limit for some flow quantities in some of the cases simulated.
 378 The hit rate q is strongly dependent on the values chosen for AD and RD . By making use of
 379 more restricted values of AD for normalised velocities, such as those used by Franke et al.
 380 (2008) ($AD=0.008$ and 0.007 for \bar{U}/U_0 , \bar{W}/U_0), the tendency of q to decrease is higher
 381 for the vertical velocity than for the streamwise velocity, see Tables 2 and 3. This behaviour
 382 is related to the very low values of \bar{W}/U_0 at the considered locations when it is difficult to
 383 fulfil the RD criterion so that a change in AD affects strongly the value of q . The dependency
 384 of q upon AD is smaller for \bar{U}/U_0 because, in general, the values of \bar{U}/U_0 are high and it is
 385 easier to fulfil the RD criterion (most of them fulfil this criterion independently of the AD
 386 value). The difficulty of setting a meaningful value of q makes it worthwhile to consider
 387 other metrics to complete the statistical analysis.

388 4.1.2 Other Metrics

389 The values of FB , $FAC2$ and $NMSE$ defined earlier are given in Tables 2 and 3. Similar to
 390 the hit rate, these values show a better fit with the experiments for the full dataset than for
 391 the data within the canopy. The positive values of FB indicate an underestimation of all flow
 392 variables by both models. In general, RANS and LES simulations have good correlation, with
 393 R close to 1 for the velocity components and around 0.7 for the Reynolds stress. The $FAC2$

and NMSE indicate a good agreement between the model results and the experimental data for the streamwise velocity and Reynolds stress but not for the vertical velocity. As for the hit rate q , the small values around zero (positive and negative) of \overline{W}/U_0 at the measurement locations means that in some cases the value of the statistical parameters is not meaningful.

Globally, LES and RANS computations give close values of hit rate and other metrics for both the streamwise velocity and Reynolds shear stress. These values indicate that both methodologies provide reasonable predictions. The vertical velocity is generally underestimated, even if LES performs better than RANS (better hit rate and FAC2).

The underestimation of \overline{W}/U_0 produced by RANS simulations is a known feature and was observed in a previous study by Olesen et al. (2008) and Franke et al. (2008) who compared the performance of various RANS models in the MUST flow configuration. A comparative analysis based on statistical metrics is helpful in estimating the errors in models, however it can lead to misleading conclusions since the experimental sample data are limited (i.e., only a few measurement locations). In the next section a comparison based on the mean flow profiles is given.

4.2 Mean Flow Field

4.2.1 Local Mean Velocity and Reynolds Stress Profiles

4.2.1.1 Regular Array Case. The profiles of the mean streamwise and vertical velocity components, \overline{U}/U_0 and \overline{W}/U_0 , and of the Reynolds shear stress, $\overline{u'w'}/U_0^2$, obtained with RANS and LES computations are compared with experimental data in Fig. 5 at different locations inside the array. Note that the experimental data are extracted from the wind-tunnel experiment by Bezpalcova (2007) for the scaled model of the MUST field configuration that incorporates the geometrical irregularities. The locations selected for the comparisons are shown in Fig. 1 for the experiment and Fig. 2a and b for the simulations. The positions SC9, SC15, L9 and L14 are well located within the array so that the influence of inflow conditions can be minimized at these locations according to Meinders and Hanjalic (1999) who showed experimentally that far downstream of the inlet of a matrix of cubes the flow was developed and periodic. The simulations provide very similar profiles of the velocity components \overline{U}/U_0 and \overline{W}/U_0 at locations SC4–SC6. Along this line the RANS shear-stress profiles exhibit as well a very similar behaviour among the locations, while the LES shear-stress profiles exhibit a peak that tends to decrease going downstream of the array. Passing through positions L4–L6, the streamwise mean velocity component shows insignificant variations. However, if the mean vertical velocity component and the shear stress present similar profile shapes, some differences in the peak values are observed among the locations, and are more pronounced in the LES case. The velocity component \overline{U}/U_0 is closer to the measurements in the LES than in the RANS. For the mean vertical velocity component, \overline{W}/U_0 , and the shear stress, $\overline{u'w'}/U_0^2$, the LES predicts higher values than RANS, the best agreement with the experiments being obtained with LES, in particular for \overline{W}/U_0 at the SC locations and $\overline{u'w'}/U_0^2$ at the L locations. A general tendency of RANS is to underestimate the vertical velocity and shear stress, in particular at L4–L6 where the values of \overline{W}/U_0 and $\overline{u'w'}/U_0^2$ are very low. Note that large discrepancies between both RANS and LES simulations and experiments are observed for \overline{W}/U_0 at the L locations. This is an effect of irregularities as will be shown in the next section.

4.2.1.2 Irregular array case. Figure 6 presents the comparisons of the mean velocity and Reynolds shear-stress profiles between the measurements and the results obtained by RANS

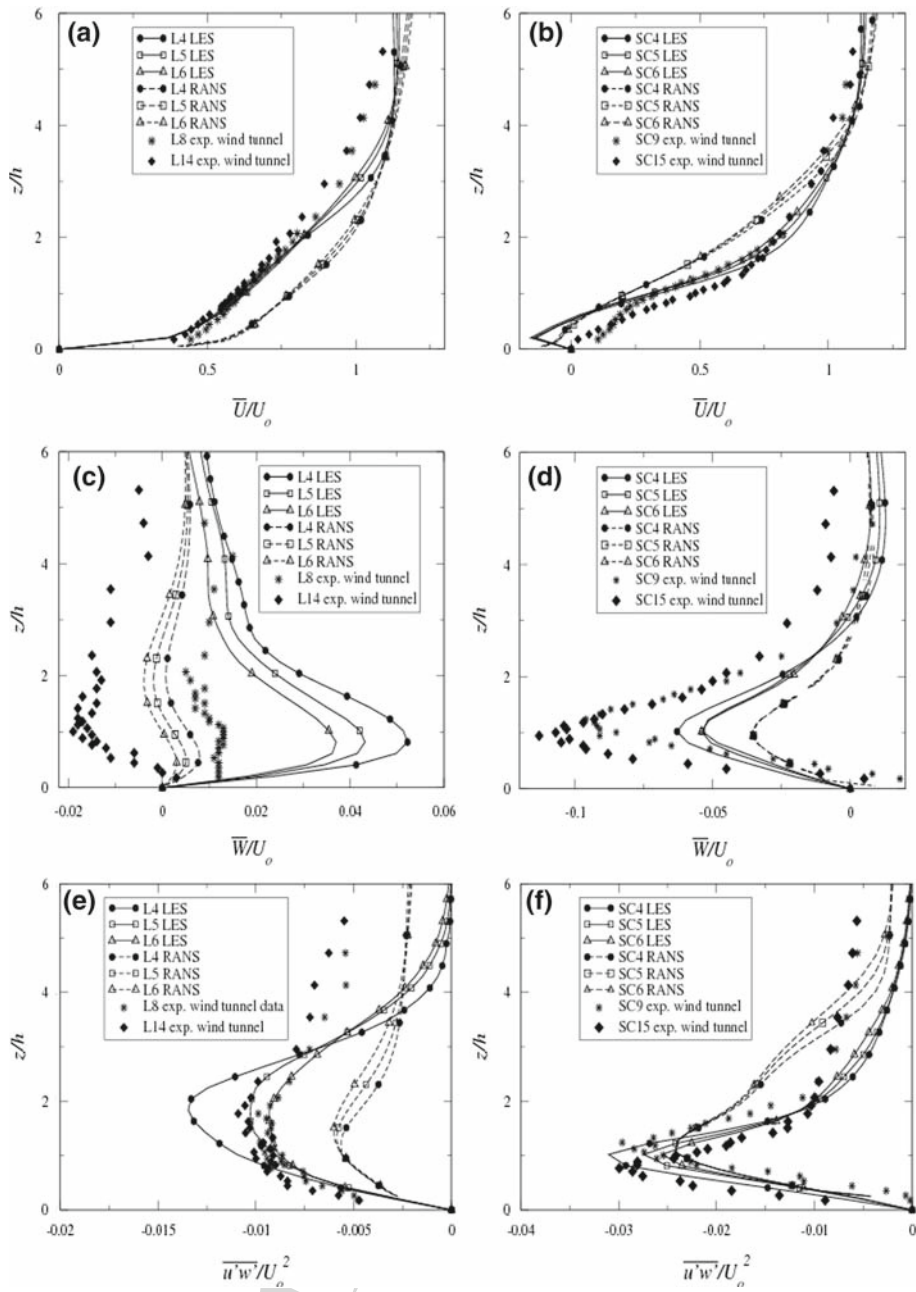


Fig. 5 Regular array simulations: **a** and **b** vertical profiles of the mean streamwise velocity, \bar{U}/U_o ; **c** and **d** vertical profiles of the mean vertical velocity, \bar{W}/U_o ; **e** and **f** vertical profiles of the Reynolds shear stress, $\overline{u'_i u'_j}/U_o^2$. Note that the wind-tunnel measurements were performed for the irregular array and that the locations are indicated in Figs. 1 and 2

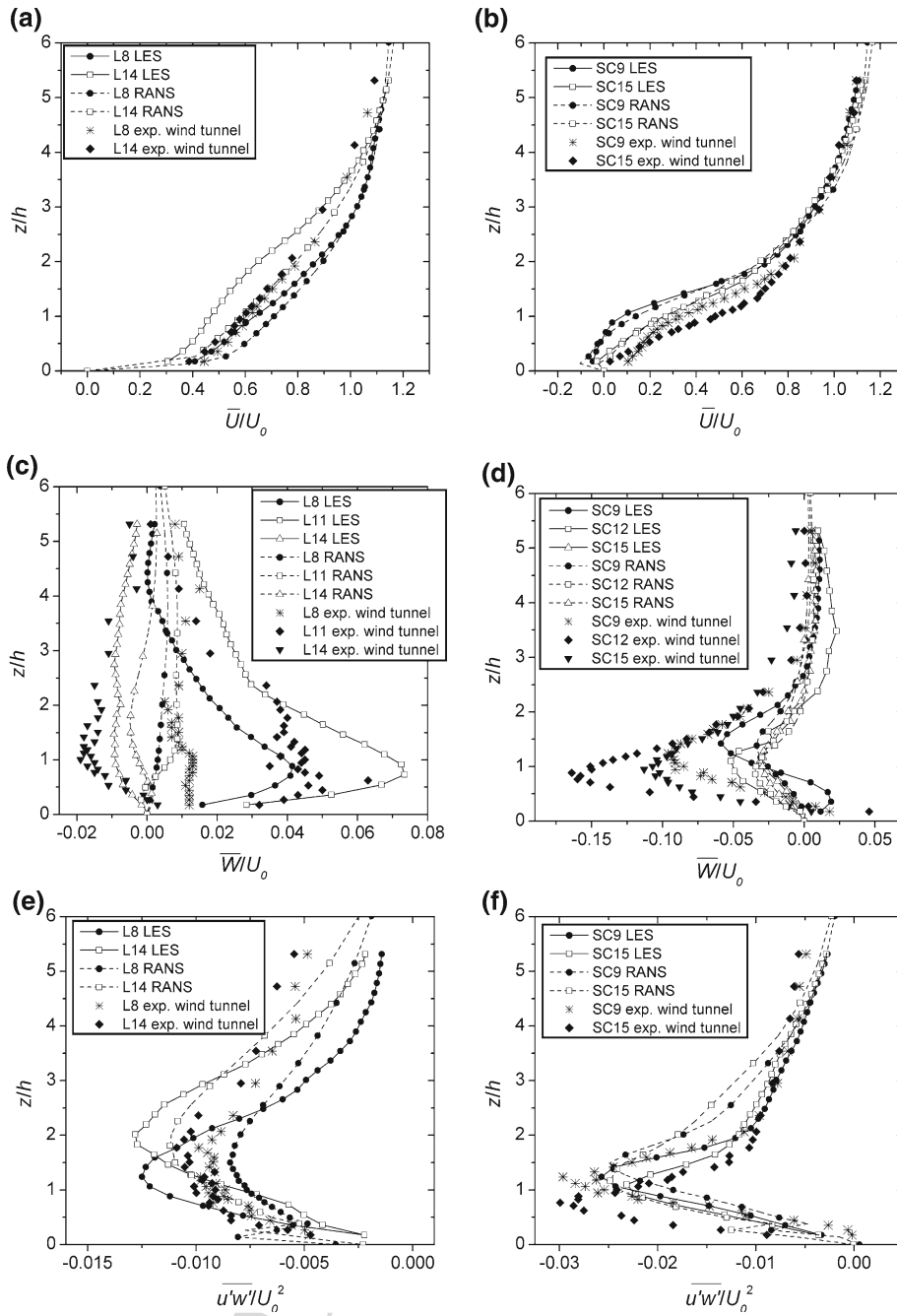


Fig. 6 Irregular array simulations; **a** and **b** vertical profiles of the mean streamwise velocity, \bar{U}/U_0 ; **c** and **d** vertical profiles of the mean vertical velocity, \bar{W}/U_0 ; **e** and **f** vertical profiles of the Reynolds shear stress, $\overline{u'w'}/U_0^2$ (see Fig. 1 for the locations)

438 and LES for the irregular array. The locations for the comparisons are shown in Fig. 1. The
 439 experimental data of \overline{U}/U_0 and $\overline{u'w'}/U_0^2$ show a small dependency on the locations SC9–SC15
 440 and L9–L15, however \overline{W}/U_0 presents a strong variation along L9–L15 while it differs very
 441 little from SC9 to SC15. Regarding the simulations, at SC9–SC15 the irregularities have little
 442 effect on the RANS and LES streamwise mean velocity and on the shear-stress profiles, and
 443 are of the same order as those from the experiment. At locations L9–L15, the simulations
 444 show a somewhat higher influence from the irregularities than the experiments for \overline{U}/U_0 .
 445 Figure 6c and d shows that LES captures better the variations of \overline{W}/U_0 than RANS, which
 446 provides values of the vertical velocity component that are too low. Regarding the other
 447 flow quantities, RANS and LES give similar results and, globally, a reasonable agreement is
 448 obtained with the measurements.

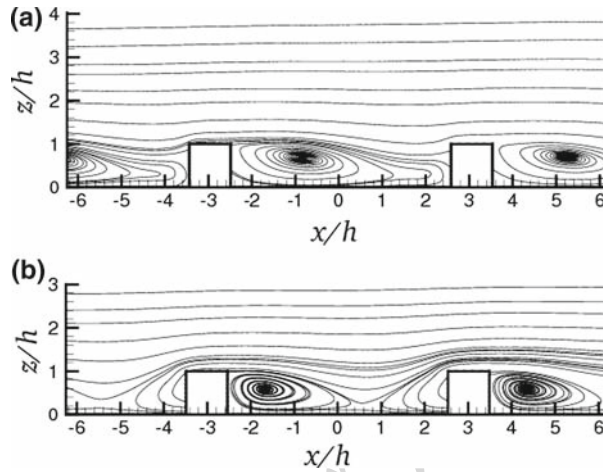
449 The comparison between the results obtained with RANS and LES for the regular and
 450 irregular cases and the experimental data (that include the geometrical irregularities) shows
 451 that the impact of the irregularity is the most significant for the vertical velocity compo-
 452 nent, especially along the L positions where the flow is channelled and the velocity profile
 453 changes in shape from one position to another. This behaviour is reasonably well predicted
 454 by LES but missed by RANS. Inside the recirculation flow regions the vertical velocity
 455 component is less affected by geometrical irregularities and the profile conserves a simi-
 456 lar shape. The streamwise velocity component and shear-stress profiles are little affected
 457 by the irregularities whatever the locations considered and for these quantities LES and
 458 RANS give similar results that are in satisfactory agreement with experiments. Regarding
 459 the mean vertical velocity, LES provides a better prediction than RANS but both mod-
 460 els show deficiencies in the overall predictions. As mentioned in the previous section,
 461 the underestimation of \overline{W}/U_0 is a common feature of RANS models (Olesen et al. 2008;
 462 Franke et al. 2008). Note that the mean vertical velocity takes small values at the con-
 463 sidered locations, so that even if the relative error is high for this velocity component,
 464 the magnitude of the absolute error is probably comparable with that for the streamwise
 465 velocity.

4.2.2 Streamlines

467 Figures 7 and 8 show the averaged streamlines on a 2D plane for the mean flow velocity field
 468 obtained from LES and RANS simulations for the regular array. The x - z plane along the line
 469 defined by the SC locations (see Fig. 2) is considered in Fig. 7 and the plane x - y at altitude
 470 $z/h = 0.5$ in Fig. 8. When comparing LES and RANS it is observed that the recirculation
 471 zone behind the containers is larger in LES than in RANS. The smaller recirculation zone
 472 found in RANS is in agreement with the results of Sini et al. (1996). In addition, Castro
 473 and Apsley (1997) observed that the k - ϵ model poorly predicts the flow impingement and
 474 separation. Note that for RANS the flow re-attaches between two containers while this is not
 475 the case for LES.

476 The streamlines obtained from the simulations of the irregular array case in the
 477 x - y plane at altitude $z/h = 0.5$ are shown in Fig. 9, where it is seen that the inclu-
 478 sion of irregularities affects the flow locally. In particular the container of different shape
 479 and size located at $x/h \approx -8$ and $y/h \approx 4$ presents smaller downward recircula-
 480 tion zones, and the non-alignment of the containers in the region $2 < x/h < 10$ and
 481 $-10 < y/h < 10$ inhibits the formation of recirculation downstream of some of the con-
 482 tainers. For this case both RANS and LES provide a similar behaviour. Again a tendency
 483 for RANS to predict smaller recirculation regions is observed. In general, the irregulari-
 484 ties tend to break the repeated characteristic of the flow patterns observed in the regular
 485 geometry.

Fig. 7 Streamlines of the mean flow velocity field for the regular case in the plane ($z-x$) along the line described by SC locations (see Fig. 2). **a** LES; **b** RANS. Note that the 2D representation of the streamlines corresponds to the lines tangent to the velocity vector field projected in the corresponding plane



486 4.3 Spatially-Averaged Properties

487 As previously mentioned, in atmospheric (mesoscale) modelling of the urban environment,
 488 the whole city and its surrounding areas cannot be simulated (for computational reasons) at a
 489 resolution high enough to explicitly capture features of the flow around individual buildings.
 490 Therefore the urban canopy layer has to be parameterised to reproduce the effects of the complex
 491 morphology of a city (buildings, cars, gardens, etc) on the atmosphere. To determine the
 492 parameters required for atmospheric models, information is needed from spatial-averaged
 493 flow properties of the urban layer. Here, spatially-averaged properties of flow field quantities
 494 obtained from the LES and RANS simulations are compared.

495 The RANS model provides time-(or ensemble-) averaged values (indicated here by an
 496 overbar) and the extraction of spatially-averaged values (indicated by $\langle \rangle$) consists of aver-
 497 aging in space the time- (or ensemble-) averaged field variables. Regarding LES, the flow
 498 quantities are first averaged in time before applying the space average.

499 The spatial average of a variable ψ can be defined as (see Martilli and Santiago 2007),

500
$$\langle \bar{\psi} \rangle = \frac{1}{V_{\text{air}}} \int_{V_{\text{air}}} \bar{\psi}(\vec{x}, t) d\vec{x} \quad (11)$$

501 where $\langle \rangle$ denotes an horizontal space average operator. The spatial average of the stream-
 502 wise and vertical velocity components, $\langle \bar{U} \rangle$ and $\langle \bar{W} \rangle$, of the Reynolds and dispersive shear
 503 stresses, $\langle \overline{u'w'} \rangle$ and $\langle \widehat{u} \widehat{w} \rangle$, are analysed as functions of vertical distance from the ground. The
 504 dispersive stress is related to the vortex formed in the street canyons (Martilli and Santiago
 505 2007) and is defined as,

506
$$\widehat{u} \widehat{w}_{ij} = (\langle \bar{u} \rangle - \bar{u}_{ij}) (\langle \bar{w} \rangle - \bar{w}_{ij}), \quad (12)$$

507 Note that, usually, the dispersive stress is denoted as $\widetilde{u} \widetilde{w}$ but here is written as $\widehat{u} \widehat{w}$ to avoid
 508 confusion with the filtered LES variables represented with a tilde (\sim).

509 The spatially-averaged flow properties are given for the regular and irregular cases. In
 510 the regular array case, the horizontal average is applied over the central street canyon unit
 511 (one building and one canyon). In this way, the effects of the array borders on the flow are
 512 smoothed and the average properties made over this region are representative of the behav-
 513 iour of the flow within the array. To also minimize border effects in the irregular array case,

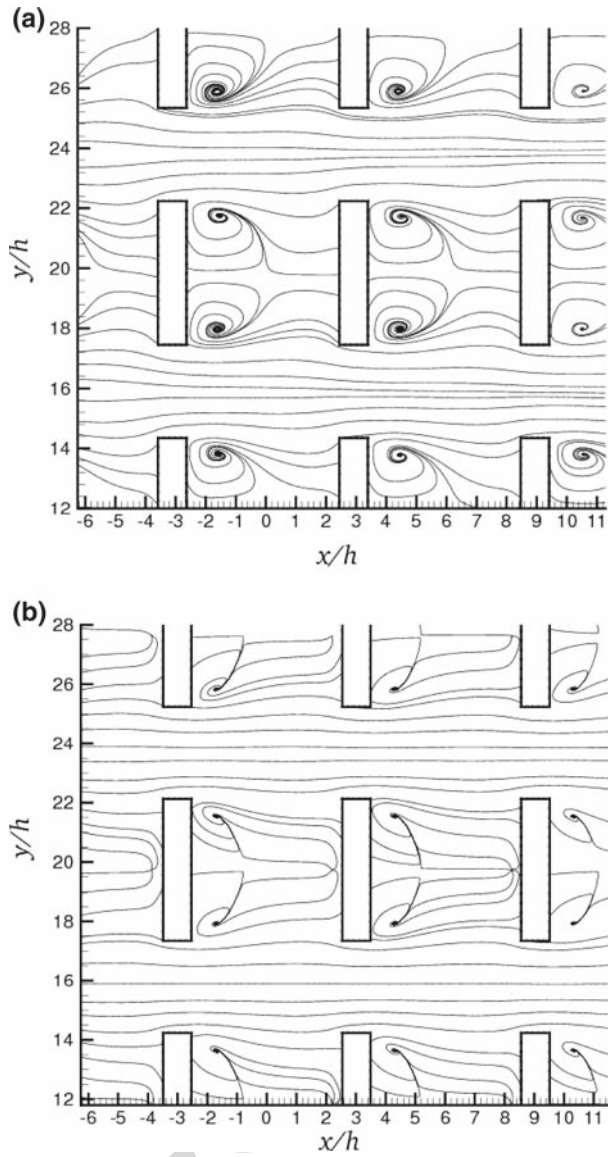
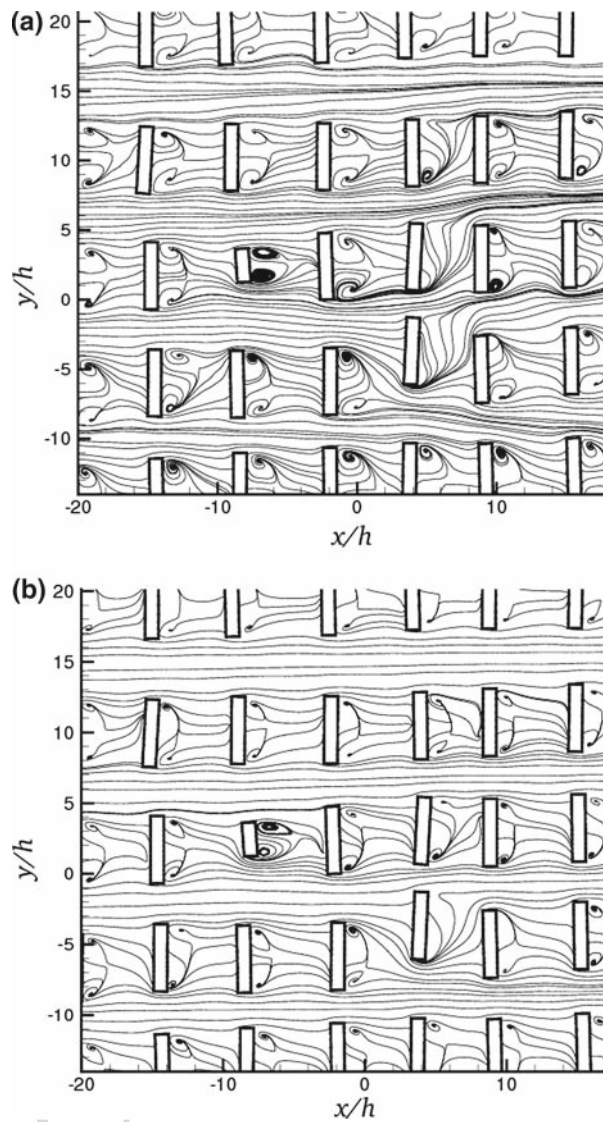


Fig. 8 Regular array simulations: streamlines of the mean flow velocity field in the plane (x - y) at $z/h = 0.5$. **a** LES; **b** RANS. Note that the 2D representation of the streamlines corresponds to the *lines* tangential to the velocity vector field projected in the corresponding plane

514 the spatial averages are performed over the whole array with the exception of the first row of
 515 building-canyon units around the array.

516 Figure 10 shows the profiles of the spatially-averaged variables $\langle \bar{U} \rangle / U_0$, $\langle \bar{W} \rangle / U_0$,
 517 $\langle \bar{u}'w' \rangle / U_0^2$ and $\langle \bar{\hat{u}} \hat{w} \rangle / U_0^2$. Only slight differences are observed in the space average proper-
 518 ties between RANS and LES for both the regular and irregular cases. The flow properties are
 519 also seen to be insignificantly modified by the presence of small irregularities. In particular,

Fig. 9 Irregular array simulations: streamlines of the mean flow velocity field in the plane $(x-y)$ at $z/h = 0.5$. **a** LES; **b** RANS. Note that the 2D representation of the streamlines corresponds to the *lines* tangential to the velocity vector field projected in the corresponding plane



520 the high spatial dependence observed on the time-averaged profile \overline{W}/U_0 (see Fig. 6c) is
 521 smoothed when the spatial average is applied. Regarding the dispersive stress, the RANS
 522 results are close to those for LES and both are found to be almost insensitive to small geo-
 523 metrical irregularities. The RANS and LES dispersive stresses are shown to be very small in
 524 comparison with the spatially-averaged shear stresses in the whole domain. Therefore, the
 525 dispersive stress can be neglected in comparison with the shear stress for this configuration
 526 from the point of view of urban canopy modelling. Note that the small values of the disper-
 527 sive stress are related to the low packing density of this configuration. As commented above,
 528 the dispersive stress is associated with the vortex formed in the street canyons (Martilli and
 529 Santiago 2007). In the present case, the aspect ratio of these street canyons, defined as the

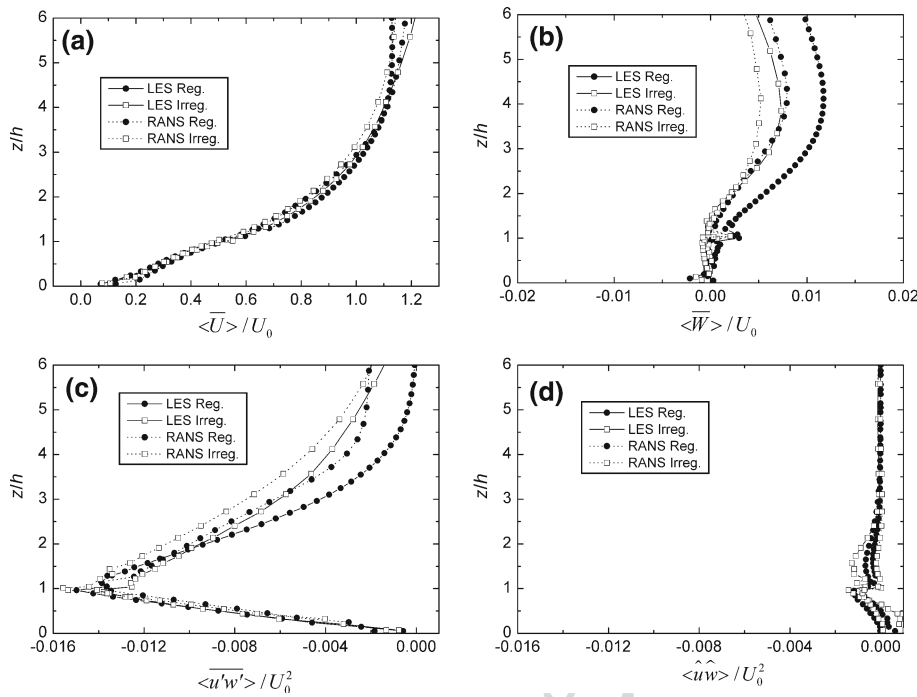


Fig. 10 Horizontal spatially-averaged flow properties: **a** vertical profiles of the mean streamwise velocity, $\langle \bar{U} \rangle / U_0$; **b** vertical profile of the mean vertical velocity, $\langle \bar{W} \rangle / U_0$; **c** vertical profiles of the Reynolds shear stress, $\langle \overline{u'w'} \rangle / U_0^2$; **d** vertical profiles of the dispersive stress, $\langle \widehat{u\bar{w}} \rangle / U_0^2$

530 ratio of the width of the street and the height of the obstacle, is approximately 5 so that the
 531 flow regime is far from the skimming flow where the contribution of the dispersive fluxes
 532 can be important inside the urban canopy (Martilli and Santiago 2007).

533 The present RANS and LES results show that the spatially-averaged flow properties are
 534 not sensitive to small geometrical irregularities (as presented here). Moreover, the spatially-
 535 averaged flow properties of a reduced array, limited to one unit container, are shown to be very
 536 similar to the flow properties averaged over the full array of containers. This suggests that one
 537 part of a city can be represented by a simplified configuration (e.g., a periodic domain of one
 538 building-street unit) when spatial averages are of interest and that, for the reduced configura-
 539 tions, the CFD models can be helpful in improving canopy models by providing properties
 540 that are difficult to obtain experimentally (e.g., the assessment of drag coefficients).

541 **5 Conclusions**

542 In this study, RANS and LES are used to simulate the flow over the MUST field experiment
 543 geometry that is representative of a simplified urban environment. In the LES simulations
 544 presented here the grid mesh resolution was chosen in order to ensure a reasonable resolution
 545 of the large-scale flow generated by the containers while keeping the computing times two
 546 orders of magnitude below those needed for RANS calculations. The aim was to investi-
 547 gate the feasibility and the potential superiority of using LES compared to RANS for the
 548 simulation of flow within urban-like geometry at a relative low computational cost.

The comparative analysis used as a reference the wind-tunnel experimental data of [Bezpalcova \(2007\)](#) for a flow configuration with an upstream flow directed perpendicular to the front of the obstacles. The comparisons were based on a statistical analysis and by comparing mean flow quantities. For the mean flow quantities, effects of small geometrical irregularities were addressed at the microscale level (building flow scales) and at the mesoscale level (space-averaged flow properties).

A statistical analysis based on various metrics proposed in the literature showed a reasonably good prediction of the mean streamwise velocity and shear stress by LES and RANS; the mean vertical velocity is in general underpredicted by both methods, the LES providing however a better hit rate and FAC2 for this velocity component. This type of analysis is helpful in estimating the errors in models, but it can lead to misleading conclusions due to the limited number of experimental data available, and, as well, to the high dependence of some parameters used in the definition of the metrics for the error assessment. The differences observed in the flow structure between the RANS and LES are shown to not affect the similarity in the hit rate between the two computational approaches so that caution should be used when interpreting this metric.

At the microscale level, small irregularities are shown to affect significantly the mean vertical velocity component while the mean streamwise velocity and Reynolds shear stress are shown to be less sensitive to small geometrical perturbations. Their inclusion also breaks the repeated flow patterns found in an array of containers with identical shape and which are perfectly aligned. For the mean streamwise velocity and Reynolds shear stress, the present LES results are found to be close to RANS results and both approaches were in satisfactory agreement with the observations. However, LES captured better the irregularity effects observed on the vertical velocity components. The magnitude of this velocity component is in general underestimated by RANS.

At the mesoscale level, the small geometrical perturbation effects were found insignificant for both the spatially-averaged streamwise and vertical velocity components and as well for the spatially-averaged Reynolds shear stress. Regarding the dispersive stress, it was shown to be negligible compared to the spatially-averaged shear stress. Globally, the results obtained with LES and RANS for the spatially-averaged flow properties were found to be similar for each flow configuration considered and only slight differences were observed in the four cases studied (LES in regular and irregular arrays, and RANS in regular and irregular arrays). At this scale level, it was shown that the flow properties averaged over the full MUST array flow configuration are similar to the flow properties averaged over the one unit regular container flow configuration. This result is very relevant from the urban canopy modelling point of view because the spatially-averaged flow properties computed by CFD models in a simplified configuration can be representative of the average properties of a real part of a city without large irregularities, and can be used for the improvement of the parameterisation of atmospheric mesoscale models.

Acknowledgements The authors wish to thank J. M. White and B. Leitl for providing field data and wind-tunnel data from the MUST experiment, respectively and J. Franke for providing one of the meshes used in this study. The present study was funded by the Spanish Ministry of Defence.

References

- Bezpalcova K (2007) Physical modelling of flow and dispersion in an urban canopy. PhD thesis, Faculty of Mathematics and Physics, Charles University, Prague, 193 pp
- Biltoft CA (2001) Customer report for Mock Urban Setting Test (MUST). DPG document WDTC-TP-01-028, West Desert Test Center, U.S. Army Dugway Proving Ground, Dugway, Utah, 58 pp

- 596 Cabot W, Moin P (1999) Approximate wall boundary conditions in the large eddy simulation of high Reynolds
597 number flow. *Flow Turbul Combust* 63:269–291
- 598 Camelli FE, Löhner R, Hanna SR (2005) VLES study of MUST experiment. In: 43rd AIAA Aerospace Meeting
599 and Exhibit, January 10–13, Reno, Nevada, paper 1279, 19 pp
- 600 Castro IP, Apsley DD (1997) Flow and dispersion over topography: a comparison between numerical and
601 laboratory data for two-dimensional flows. *Atmos Environ* 31:839–850
- 602 Castro IP, Robins AG (1997) The flow around a surface-mounted cube in uniform and turbulent streams.
603 *J Fluid Mech* 79:307–335
- 604 Castro IP, Cheng H, Reynolds R (2006) Turbulence over urban-like roughness: deductions from wind-tunnel
605 measurements. *Boundary-Layer Meteorol* 118:109–131
- 606 Cheng H, Castro IP (2002) Near wall flow over urban-like roughness. *Boundary-Layer Meteorol* 104:229–259
- 607 Cheng Y, Lien FS, Yee E, Sinclair R (2003) A comparison of large eddy simulations with a standard $k-\epsilon$
608 Reynolds-averaged Navier–Stokes model for the prediction of a fully developed turbulent flow over a
609 matrix of cubes. *J Wind Eng Ind Aerodyn* 91:1301–1328
- 610 Coceal O, Belcher SE (2004) A canopy model of mean winds through urban areas. *Q J Roy Meteorol Soc*
611 130:1349–1372
- 612 Coceal O, Thomas TG, Castro IP, Belcher SE (2006) Mean flow and turbulence statistics over groups urban-
613 like cubical obstacles. *Boundary-Layer Meteorol* 121:491–519
- 614 Dejoan A, Santiago JL, Martilli A, Martin F, Pinelli A (2010) Comparison between LES and RANS compu-
615 tations for the MUST field experiment. Part II: effects of incident wind deviation angle on the mean flow
616 and plume dispersion. *Boundary-Layer Meteorol* (in press)
- 617 Di Sabatino S, Buccolieri, Olesen H, Ketzel M, Berkowicz R, Franke J, Schatzmann M, Schlünzen H,
618 Leitl B, Britter R, Borrego C, Costa AM, Trini-Castelli S, Reisin T, Hellsten A, Saloranta J, Mousi-
619 siopulos N, Barmpas F, Brzozowski K, Goricsan I, Balczò M, Bartzis J, Efthimiou G, Santiago JL,
620 Martilli A, Piringer M, Hirtl M, Baklanov A, Nuterman R, Starchenko A (2009) COST 732: in practice:
621 the MUST model evaluation exercise. *Int J Environ Pollut* (in press)
- 622 Dobre A, Arnold SJ, Smalley RJ, Boddy JWD, Barlow JF, Tomlin AS, Belcher SE (2005) Flow field mea-
623 surements in the proximity of an urban intersection in London, UK. *Atmos Environ* 39:4647–4657
- 624 Eichhorn J (2004) Application of a new evaluation guideline for microscale flow models. In: 9th interna-
625 tional conference on harmonisation within atmospheric dispersion modelling for regulatory purposes,
626 Garmisch-Partenkirchen, June 1–4, Germany, 5 pp
- 627 Flaherty JE, Stock D, Lamb B (2007) Computational fluid dynamic simulations of plume dispersion in urban
628 Oklahoma City. *J Appl Meteorol Clim* 46:2110–2126
- 629 Fluent Inc. (2005) FLUENT 6.2 User's guide, vols 1–3. Fluent Inc., Lebanon, 2216 pp
- 630 Franke J, Bartzis J, Barmpas F, Berkowicz R, Brzozowski K, Buccolieri R, Carissimo B, Costa A,
631 Di Sabatino S, Efthimiou G, Goricsan I, Hellsten A, Ketzel M, Leitl B, Nuterman R, Olesen H,
632 Polreich E, Santiago JL, Tavares R (2008) The MUST model evaluation exercise: statistical analysis
633 of modelling results. In: 12th international conference on harmonisation within atmospheric dispersion
634 modelling for regulatory purposes, Cavtat, October 6–9, Croatia, 5 pp
- 635 Hanna SR, Tehrani S, Carissimo B, Macdonald RW, Löhner R (2002) Comparisons of model simulations
636 with observations of mean flow and turbulence within simple obstacle arrays. *Atmos Environ* 36:5067–
637 5079
- 638 Kastner-Klein P, Plate EJ (1999) Wind-tunnel study of concentration fields in street canyons. *Atmos Environ*
639 33:3973–3979
- 640 Kim JJ, Baik JJ (2004) A numerical study of effects of ambient wind direction on flow and dispersion in urban
641 street canyons using the RNG $k-\epsilon$ turbulence model. *Atmos Environ* 38:3039–3048
- 642 Launder BE, Spalding DB (1974) The numerical computation of turbulent flow. *Comput Method Appl Mech*
643 3:269–289
- 644 Leitl B, Bezpalcova K, Harms F (2007) Wind Tunnel Modelling Of The MUST Experiment. In: 11th interna-
645 tional conference on harmonisation within atmospheric dispersion modelling for regulatory purposes,
646 Cambridge, July 2–5, UK, 5 pp
- 647 Lim HC, Castro IP, Hoxey RP (2007) Bluff bodies in deep turbulent boundary layers: Reynolds-number issues.
648 *J Fluid Mech* 571:97–118
- 649 Martilli A, Santiago JL (2007) CFD simulation of airflow over a regular array of cubes. Part II: analysis of
650 spatial average properties. *Boundary-Layer Meteorol* 122:635–654
- 651 Martilli A, Clappier A, Rotach MW (2002) An urban surface exchange parameterization for mesoscale models.
652 *Boundary-Layer Meteorol* 104:261–304
- 653 Meinders ER, Hanjalic K (1999) Vortex structures and heat transfer in turbulent flow over a wall-mounted
654 matrix of cubes. *Int J Heat Fluid Flow* 20:255–267
- 655 Meroney RN, Pavegeau M, Rafailidis S, Schatzmann M (1996) Study of line source characteristics for 2D
656 physical modelling of pollutant dispersion in street canyons. *J Wind Eng Ind Aerodyn* 62:37–56

- 657 Michioka M, Sato A (2009) Numerical simulations of gas dispersion in a residential area. In: The seventh
 658 international conference on urban climate, Yokohama, June 29-July 3, Japan, 4 pp
- 659 Milliez M, Carissimo B (2007) Numerical simulations of pollutant dispersion in an idealized urban area for
 660 different meteorological conditions. *Boundary-Layer Meteorol* 122:321–342
- 661 Nikitin NV, Nicoud F, Wasistho B, Squires KD, Spalart PR (2000) An approach to wall modelling in large
 662 eddy simulation. *Phys Fluids* 12:1629–1632
- 663 Olesen HR, Baklanov A, Bartzis J, Barmpas F, Berkowicz R, Brzozowski K, Buccolieri R, Carissimo B, Costa
 664 A, Di Sabatino S, Efthimiou G, Franke J, Goricsan I, Hellsten A, Ketzel M, Leidl B, Nuterman R, Polreich
 665 E, Santiago J, Tavares R (2008) The MUST model evaluation exercise: patterns in model performance. In:
 666 12th international conference on harmonisation within atmospheric dispersion modelling for regulatory
 667 purposes, Cavtat, October 6–9, Croatia, 5 pp
- 668 OpenFoam (2006) Version 1.3, User and Programmer guide. Technical Report. <http://www.openfoam.com/>
 669 [openfoam](http://www.openfoam.com/)
- 670 Patankar SV (1980) Numerical heat transfer and fluid flow. Hemisphere Publishing Corporation, New York,
 671 197 pp
- 672 Pavageau M, Schatzmann M (1999) Wind tunnel measurements of concentration fluctuations in an urban street
 673 canyon. *Atmos Environ* 33:3961–3971
- 674 Piomelli U, Ballaras E (2002) Wall-layer models for Large Eddy Simulations. *Annu Rev Fluid Mech* 34:349–
 675 374
- 676 Santiago JL, Martilli A, Martin F (2007) CFD simulation of airflow over a regular array of cubes. Part I: three-
 677 dimensional simulation of the flow and validation with wind-tunnel measurements. *Boundary-Layer*
 678 *Meteorol* 122:609–634
- 679 Santiago JL, Coceal O, Martilli A, Belcher SE (2008) Variation of the sectional drag coefficient of a group of
 680 buildings with packing density. *Boundary-Layer Meteorol* 128:445–457
- 681 Sini JF, Anquetin S, Mestayer PG (1996) Pollutant dispersion and thermal effects in urban street canyons.
 682 *Atmos Environ* 30:2659–2677
- 683 Smagorinsky J (1963) General circulation experiments with the primitive equations. *Mon Weather Rev*
 684 91(3):99–164
- 685 Smorlakiewicz PK, Sharman R, Weil J, Perry SGc, Heist D, Bowker G (2007) Building resolving large-eddy
 686 simulations and comparison with wind tunnel experiments. *J Comput Phys* 227:633–653
- 687 Snyder W (1981) Guidelines for fluid modelling of atmospheric dispersion. Report Number EPA-600/8-81-
 688 009, Environmental Protection Agency, Research Triangle Park, NC, 200 pp
- 689 Tseng Y-H, Meneveau C, Parlange M (2006) Modeling flow around bluff bodies and predicting urban disper-
 690 sion using large eddy simulation. *Environ Sci Technol* 40:2653–2662
- 691 VDI (2005) Environmental meteorology—prognostic microscale windfield models—evaluation for flow
 692 around buildings and obstacles. VDI guidelines 3783, Part 9, Beuth, Berlin
- 693 Versteeg HK, Malalasekera W (1995) An introduction to computational fluid dynamics. The finite volume
 694 method. Person Prentice Hall, Harlow, 272 pp
- 695 Xie Z, Castro IP (2006) LES and RANS for turbulent flow over arrays of wall-mounted obstacles. *Flow Turbul*
 696 *Combust* 76:291–312
- 697 Xie Z, Castro IP (2009) Large-eddy simulation for flow and dispersion in urban streets. *Atmos Environ*
 698 43:2174–2185
- 699 Yakhot A, Anor T, Liu H, Nikitin N (2006) Direct numerical simulation of turbulent flow around a wall-
 700 mounted cube: spatio-temporal evolution of large-scale vortices. *J Fluid Mech* 566:1–9
- 701 Yee E, Biltoft CA (2004) Concentration fluctuation measurements in a plume dispersing through a regular
 702 array of obstacles. *Boundary-Layer Meteorol* 111:363–415
- 703 Yee E, Gailis RM, Hill A, Hilderman T, Kiel D (2006) Comparison of wind tunnel and water-channel simu-
 704 lations of plume dispersion through a large array of obstacles with a scales field experiment. *Boundary-*
 705 *Layer Meteorol* 121:389–432